Molecular bases of cytoskeleton plasticity during the Trypanosoma brucei parasite cycle.

Brice Rotureau, Ines Subota, Philippe Bastin

▶ **To cite this version:**

Brice Rotureau, Ines Subota, Philippe Bastin. Molecular bases of cytoskeleton plasticity during the Trypanosoma brucei parasite cycle.. Cellular Microbiology, 2011, 13 (5), pp.705-16. 10.1111/j.1462-5822.2010.01566.x . pasteur-01371324

HAL Id: pasteur-01371324

https://pasteur.hal.science/pasteur-01371324v1

Submitted on 25 Sep 2016

HAL is a multi-disciplinary open access archive for the deposit and dissemination of scientific research documents, whether they are published or not. The documents may come from teaching and research institutions in France or abroad, or from public or private research centers.

L'archive ouverte pluridisciplinaire **HAL**, est destinée au dépôt et à la diffusion de documents scientifiques de niveau recherche, publiés ou non, émanant des établissements d'enseignement et de recherche français ou étrangers, des laboratoires publics ou privés.

Distributed under a Creative Commons Attribution - NonCommercial - NoDerivatives 4.0 International License

Cellular Microbiology (2011) **13**(5), 705–716
doi:10.1111/j.1462-5822.2010.01566.x
First published online 18 January 2011

Molecular bases of cytoskeleton plasticity during the *Trypanosoma brucei* parasite cycle

Brice Rotureau,* Ines Subota and Philippe Bastin
Institut Pasteur, Trypanosome Cell Biology Unit, Paris, France.

Summary

African trypanosomes are flagellated protozoan parasites responsible for sleeping sickness and transmitted by tsetse flies. The accomplishment of their parasite cycle requires adaptation to highly diverse environments. These transitions take place in a strictly defined order and are accompanied by spectacular morphological modifications in cell size, shape and positioning of organelles. To understand the molecular bases of these processes, parasites isolated from different tissues of the tsetse fly were analysed by immunofluorescence with markers for specific cytoskeleton components and by a new immunofluorescence-based assay for evaluation of the cell volume. The data revealed striking differences between proliferative stages found in the midgut or in the salivary glands and the differentiating stage occurring in the proventriculus. Cell proliferation was characterized by a significant increase in cell volume, by a pronounced cell elongation marked by microtubule extension at the posterior end, and by the production of a new flagellum similar to the existing one. In contrast, the differentiating stage found in the proventriculus does not display any increase in cell volume neither in cell length, but is marked by a profound remodelling of the posterior part of the cytoskeleton and by changes in molecular composition and/or organization of the flagellum attachment zone.

Introduction

African trypanosomes are protozoan parasites responsible for human African trypanosomiasis or sleeping sickness, a fatal tropical disease in the absence of treatment. They also infect cattle with major socio-economic consequences, mainly in east Africa (Simarro *et al.*, 2008). *Trypanosoma brucei* parasites are exclusively transmitted by the bite of the tsetse fly. In the mammalian host, trypanosomes develop in the bloodstream as extracellular parasites, and at later stages of infection, they can cross the blood–brain barrier and provoke severe neurological symptoms ultimately leading to death (Brun *et al.*, 2009). There is currently no vaccine available whereas drug treatments are difficult to apply in the field and have severe side-effects (Brun *et al.*, 2009).

A tsetse fly gets infected when it picks up trypanosomes during a blood meal on an infected mammal. To be infective for humans, parasites need to reach the tsetse saliva and to transform into the so-called metacyclic stage. This is not direct and requires several intermediate stages taking place in a strictly defined chronological order at different locations in the midgut, proventriculus and foregut, and finally in the salivary glands of the tsetse fly (Vickerman *et al.*, 1988; Roditi and Lehane, 2008) (Fig. 1). This requires specific adaptation to the varying environment, involving metabolism, cell surface proteins or striking morphological modifications (Vickerman *et al.*, 1988; Fenn and Matthews, 2007).

Trypanosomes possess a nucleus (N) and a single mitochondrion whose genetic material is condensed in a structure named kinetoplast (K) that is linked to the basal body apparatus of the flagellum (Robinson and Gull, 1991). The flagellum is attached to the cell body and tracts the trypanosome forward, hence defining the anteroposterior axis of the cell. Two main characteristic morphotypes have been defined according to the relative position of the kinetoplast to the nucleus (Hoare and Wallace, 1966). In trypomastigotes, the kinetoplast localizes between the nucleus and the posterior end of the cell. The two bloodstream forms found in mammals are the dividing slender trypomastigote and the non-dividing tsetse-infective stumpy trypomastigote that is observed at peaks of parasitaemia. After ingestion, stumpy parasites rapidly differentiate into procyclic trypomastigotes in the posterior midgut of the fly where they multiply (Fig. 1). Then, some of these procyclic parasites elongate and migrate to the anterior part of the midgut as non-proliferative mesocyclic trypomastigotes (Fig. 1). Once in the proventriculus, mesocyclic cells become thinner and adopt an epimastigote configuration, defined by the localization of the kinetoplast between the nucleus and the anterior end of the

Received 19 October, 2010; revised 25 November, 2010; accepted 7 December, 2010. *For correspondence. E-mail rotureau@pasteur.fr; Tel. (+33) 1 40 61 38 33; Fax (+33) 1 40 61 38 25.

© 2011 Blackwell Publishing Ltd

A

Morphotype	Stage	Parasite cycle → Mammalian host: Blood	Tsetse fly vector: Midgut	Tsetse fly vector: Proventriculus and foregut	Tsetse fly vector: Salivary glands
Trypomastigote	Slender *	SL			
	Stumpy	ST	ST		
	Procyclic *		PC		
	Mesocyclic		MS	MS	
Epimastigote	Dividing *			DE	
	Long			LE	
	Short			SE	SE
	Attached *				AE
Trypomastigote	Metacyclic				MT

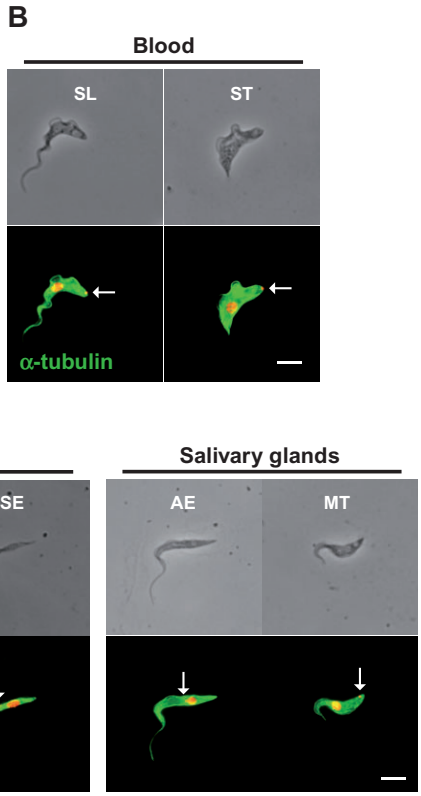

Fig. 1. Morphological changes in trypanosomes during the parasite cycle.
A. Simplified table showing the localization of each stage during the parasite cycle. Proliferative stages are indicated with *. ST, MS and SE in white boxes are only found transiently in the specified organs.
B–C. The 10 main morphological stages of the *T. brucei* parasite cycle, found in the mammalian bloodstream (B) and in the tsetse fly vector (C), were fixed in methanol and stained with DAPI (red) and the TAT1 antibody (green) recognizing α-tubulin. The α-tubulin is homogeneously distributed at the cell periphery in all stages. The scale bar represents 5 μm and the old (arrow) and new (arrowhead) basal body positions are indicated.
All stages are presented in a chronological order and the following name code has been used throughout the legends. SL: slender trypomastigote; ST: stumpy trypomastigote; PC: procyclic trypomastigote; MS: mesocyclic trypomastigote; E: proventricular epimastigote; DE: asymmetrically dividing epimastigote; LE: long epimastigote; SE: short epimastigote; AE: attached epimastigote; MT: metacyclic trypomastigote.

cell. This is due to the posterior migration of the nucleus to the other side of the kinetoplast (Sharma *et al.*, 2008). These long spermatozoa-like epimastigotes divide asymmetrically in the proventriculus and foregut to produce a long and a short epimastigote (Van Den Abbeele *et al.*, 1999) (Fig. 1). It has been proposed that, once in the salivary glands, the latter parasites attach to the epithelium via their flagellum and elongate (Sharma *et al.*, 2009) (Fig. 1). Finally, parasites adopt again the trypomastigote configuration when they transform into the metacyclic form and become competent for infecting mammalian hosts upon release in the saliva.

Parasite proliferation is encountered in three different situations: in the bloodstream (slender stage), in the midgut (procyclic stage) and in the salivary glands (attached epimastigotes). The progression of trypanosomes in the cell cycle can be monitored by a simple DNA staining as cells with one kinetoplast and one nucleus (1K1N) are in the G1/S phase, those with two kinetoplasts and one nucleus (2K1N) are in G2/M, and individuals with two kinetoplasts and two nuclei (2K2N) are about to undergo cytokinesis (Sherwin and Gull, 1989a; Woodward and Gull, 1990). Cellular and molecular information about cytoskeleton organization, composition and evolution during the cell cycle have been obtained from studies mostly carried out on the cultured procyclic form of the parasite (Gull, 1999; Ralston *et al.*, 2009). In trypanosomes, the shape of the cell is defined by a peripheral corset of microtubules that are cross-linked to each other and to the plasma membrane (Sherwin and Gull, 1989a). All these microtubules have the same polarity with their positive end at the posterior part of the cell (Robinson *et al.*, 1995). The flagellum is attached along most of the length of the cell body where a complex structure called the flagellum attachment zone (FAZ) is present. The FAZ has been defined as comprising the FAZ filament present in a gap between two microtubules of the corset, and the specialized microtubule quartet, associated to the smooth

endoplasmic reticulum (Robinson *et al*., 1995). Its elongation is co-ordinated with that of the flagellum (Kohl *et al*., 1999). From observation of procyclic parasites in culture, the FAZ has been proposed to control cell division by defining the cleavage furrow for cytokinesis (Robinson *et al*., 1995). The positioning of the new flagellum is defined by the flagella connector, a short pyramidal structural that connects the tip of the new flagellum to the side of the old flagellum (Moreira-Leite *et al*., 2001). Restricting the elongation of only the new flagellum by inactivation of intraflagellar transport is accompanied by the construction of a shorter FAZ filament, whose length is correlated with that of the new flagellum (Kohl *et al*., 2003). When such cells divide, the progeny inheriting the new flagellum is shorter, with a direct correlation between cell size and flagellum and FAZ length (Kohl *et al*., 2003). This is accompanied by a failure in basal body migration (Davidge *et al*., 2006; Absalon *et al*., 2007).

To understand the molecular bases of the numerous morphological changes occurring during the parasite cycle (Van Den Abbeele *et al*., 1999; Sharma *et al*., 2008; 2009), we have investigated the evolution of key cytoskeleton components *in vivo* using a panel of specific molecular markers for the sub-pellicular microtubules, the flagellum and the FAZ. A new immunofluorescence-based assay for evaluation of the cell volume with 3D reconstruction was developed. We reveal that whereas the three proliferative stages exhibit common points in terms of cytoskeletal rearrangements during their cell cycle, the transition from the procyclic trypomastigote to the short epimastigote form in the proventriculus and foregut happens very differently. The FAZ filament is partially remodelled, concomitantly with the migration of the nucleus towards the posterior end. Strikingly, the entire sub-pellicular microtubule cytoskeleton of the future short epimastigote daughter cell appears to be remodelled before the asymmetric division, a phenomenon that takes place without visible modification of the cell volume.

Results

To investigate cytoskeleton dynamics during trypanosome development in the tsetse fly, a total of 3992 *Glossina morsitans morsitans* tsetse flies were infected with cultured *Trypanosoma brucei brucei* strain AnTat1.1 parasites in 49 separate experiments. Out of the 761 flies dissected $\geq$ 14 days post-ingestion, 36.5% were carrying trypanosomes in the midgut and 13.5% presented infection of the salivary glands. These results indicate that the infection reached maturity in 37.1% of the infected flies. Phase-contrast microscopy coupled to 4,6-diamidino-2-phenylindole (DAPI) staining of nuclear and mitochondrial DNA confirmed the validity of the experimental set-up as all the reported parasite stages were detected upon fly dissection (Fig. 1).

Dynamics of the cytoskeleton during the parasite cycle

Overall, the total length of the parasite measured from the tip of the flagellum to the posterior end of the cell ranged from 11.5 $\pm$ 2.0 μm in short epimastigotes up to 35.3 $\pm$ 4.9 μm in epimastigotes found in the proventriculus (mean $\pm$ SD, Table S1). To understand the molecular mechanisms underlying these extensive variations of the cytoskeleton, we first monitored the distribution of sub-pellicular microtubules upon staining with the monoclonal antibody TAT1 that recognizes α-tubulin (Woods *et al*., 1989). The antibody produced a bright signal underlying the plasma membrane in all stages (Fig. 1). This was exploited to estimate the cell volume by *in silico* 3D reconstruction of confocal z-stack pictures of α-tubulin-labelled parasites (Fig. 2). In parallel, microtubule dynamics was investigated using the monoclonal antibody YL1/2 (Kilmartin *et al*., 1982) that stains tyrosinated α-tubulin and is a recognized marker of new tubulin assembly (Sherwin *et al*., 1987; Sherwin and Gull, 1989b) (Figs 3A–D and S1).

The cell volume of 1K1N parasites varied from 20 $\pm$ 3 μm^3 in short epimastigotes up to 65 $\pm$ 8 μm^3 in mesocyclic trypomastigotes (mean $\pm$ SD, Fig. 2A). Variations in cell volume between two consecutive stages were somehow correlated with those in cell length but far from direct (Fig. 2B). During the transition from the slender to the stumpy bloodstream form, the decrease in cell length (–16%) was accompanied by an increase in cell volume (+18%), with limited insertion of new tubulin at the posterior end, suggesting a rearrangement of the existing microtubules (Figs 2B and S1). In the posterior midgut of the vector, the differentiation from the stumpy to the procyclic form (Figs 2B and S1) was marked by an important elongation of the posterior end (+42%) but only a discrete increase in cell volume (+7%). Then, during the transition to the mesocyclic stage, an intense microtubule polymerization activity was detected at the tip of the flagellum and at the posterior end of cells (Fig. S1). This was accompanied by an increase in cell volume (+8 μm^3/+14%) and a lengthening of the cell (+8.9 μm/+30%), suggesting that mesocyclic parasites become thinner (Fig. 2B).

The next step of the parasite cycle is the trypomastigote to epimastigote differentiation occurring in the anterior midgut and during which both the cell length and volume remained relatively constant (Fig. 2B). After migration of the long thin nucleus towards the posterior side of the kinetoplast, the cell became very narrow while the duplicated kinetoplasts began to divide, as shown by the presence of two basal bodies labelled by

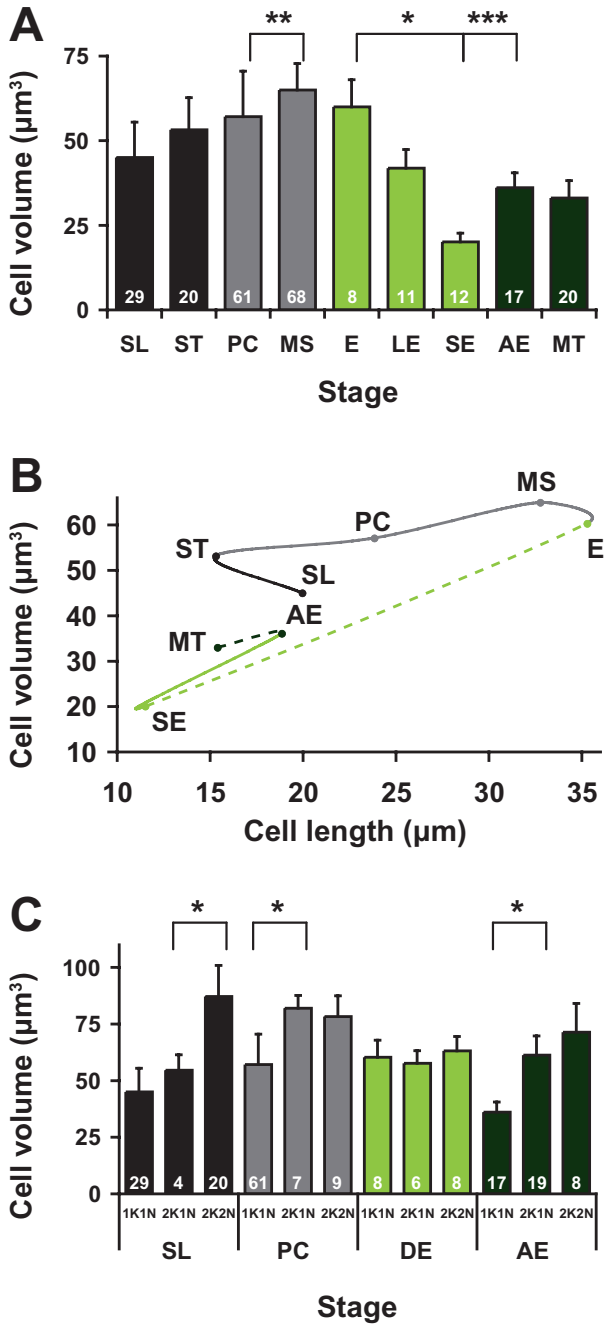

Fig. 2. Cell volume variation during the parasite cycle. The 10 main morphological stages of the *T. brucei* parasite cycle (A) and the four dividing forms (C) were fixed in PFA and stained with DAPI and the TAT1 antibody recognizing α-tubulin. The cell volume was calculated after 3D reconstruction of 200 nm confocal z-stack pictures. The number of cells studied is shown inside each column. An ANOVA test was performed and significant comparisons between two consecutive stages by Tukey *ad hoc* post-tests were indicated on the histogram with $*P < 0.0001$, $**P < 0.001$ or $***P < 0.01$.

A. Mean cell volumes ± SD (µm³) of 1K1N cells at each stage of the parasite cycle.

B. Variations of the mean cell volume ± SD (µm³) ($n = 246$) as a function of the mean total cell length ± SD (µm) of each stage ($n = 1273$). Full lines stand for differentiations and dotted lines for asymmetric divisions.

C. Mean cell volumes ± SD (µm³) of 1K1N, 2K1N and 2K2N cells in each of the four dividing stages of the parasite cycle. Stages are presented in a chronological order and the name code is given in Fig. 1.

the YL1/2 antibody (Figs 3A–D and S2). Surprisingly, binucleated epimastigotes displayed a unique YL1/2 staining pattern as the signal completely encompassed the two nuclei, corresponding to the dilated posterior part of the cell (Fig. 3B). This was further confirmed by detailed confocal observations of dividing epimastigotes using 200 nm optical sections that revealed a bright fluorescent signal drawing the entire posterior part of the cell (Figs 3E and S2). After asymmetric cell division, the staining was restricted to the tip of the flagellum, the basal body and the far posterior end of both long (Fig. 3C) and short (Fig. 3D) epimastigote cells. In contrast to the YL1/2 staining, the pattern of acetylated tubulin (Schneider *et al.*, 1987) followed faithfully the global shape of the cell, including the anterior part, as in all the other stages of the parasite cycle (Fig. S2). These results indicate an active remodelling of the posterior part of the microtubule corset concomitant to nuclear mitosis in dividing epimastigotes.

To correlate these modifications of the peripheral microtubule corset with morphological changes, the evolution of the cell volume during the cell cycle was first monitored in all three proliferating stages of the parasite cycle (bloodstream long slender, midgut procyclic and attached epimastigote in the salivary glands), and then compared with the proventricular dividing epimastigote form. A significant increase in cell volume was observed in all three proliferative stages in correlation with cell elongation (Fig. 2C). In sharp contrast, the cell volume of the epimastigotes found in the proventriculus and foregut remained constant at every step of their existence at 60 ± 8 µm³, no matter the stage of the cell cycle (from 1K1N to 2K2N, Fig. 2C). The asymmetric division resulted in the net production of a long epimastigote (42 ± 6 µm³) and a short epimastigote cell (20 ± 3 µm³).

The probable transition from this short epimastigote to the parasite attached to the salivary gland was then accompanied by a significant increase in cell volume, close to a doubling (+16 µm³/+80%), and by an important elongation of the posterior end (+7.3 µm/+48%) (Fig. 2B). Finally, trypomastigote metacyclic cells were found to be slightly smaller than their epimastigote precursors (Fig. 2B). These data reveal striking differences in the mechanisms involved in morphological modifications between proliferative stages and the differentiating stage in the proventriculus.

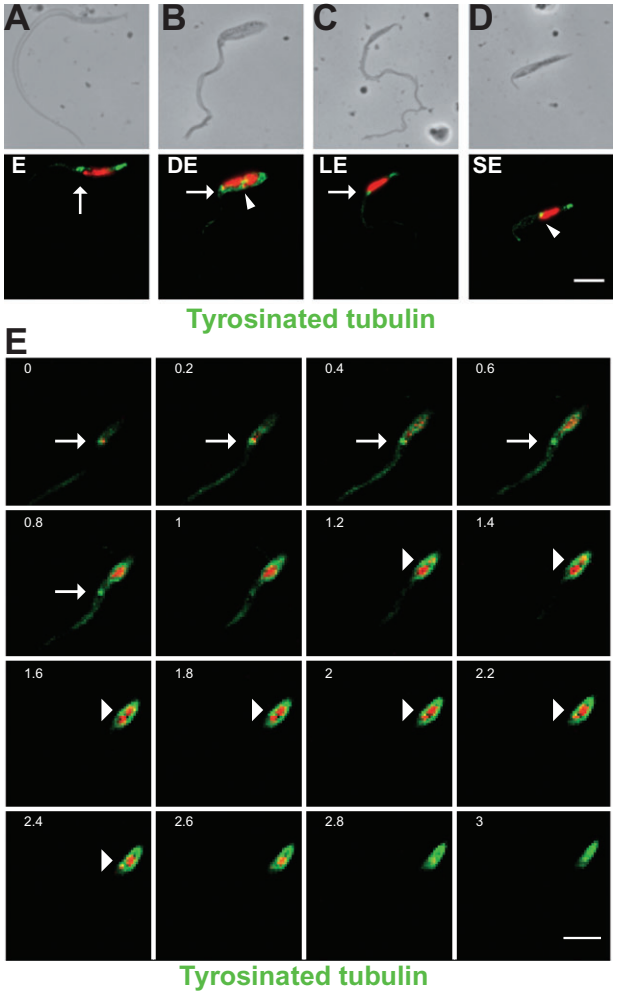

Fig. 3. Cytoskeleton remodelling during the asymmetric division in the proventriculus. Proventricular cells were fixed in methanol (A–D) or in PFA (E) and stained with DAPI (red) and the YL1/2 antibody (green) recognizing tyrosinated tubulin.
A–D. Whereas tyrosinated tubulin is found at the posterior end and the basal body of epimastigotes (A), long epimastigotes (C) and short epimastigotes (D), an intense signal was present in a larger posterior region engulfing the two nuclei in dividing epimastigotes (B). Stages are presented in a chronological order and the name code is given in Fig. 1.
E. A z-stack confocal observation of a 2K2N dividing epimastigote labelled with YL1/2 was represented from the bottom (anterior end) to the top (posterior end). A bright fluorescent signal is found around the entire peripheral microtubule corset of the future short epimastigote. The scale bars represent 5 μm and the old (arrow) and new (arrowhead) basal body positions are indicated.

Flagellum/FAZ evolution during the trypanosome parasite cycle

Because the flagellum has been shown to participate to cell morphogenesis (Robinson *et al*., 1995; Kohl *et al*., 2003; Vaughan, 2010), we monitored the evolution of typical molecular markers using the monoclonal antibodies MAb25 (Pradel *et al*., 2006) (data not shown) and L8C4 (Kohl *et al*., 1999) (Fig. S3), respectively, labelling the axoneme and the paraflagellar rod, an extra-axonemal structure that runs alongside the axoneme [review in (Portman and Gull, 2009)]. Immunofluorescence produced a clear signal throughout the length of the flagellum in all stages analysed. The length of the flagellum was measured either from the phase contrast picture or from immunofluorescence images obtained upon MAb25 or L8C4 staining (Fig. S3 and Table S1). The three sets of data correlated well, with slightly shorter values for PFR2 as expected from the position of the PFR that is only present when the flagellum exits from the flagellar pocket (Fig. S3). Flagellum length ranged from only 2.9 ± 0.6 μm in the short epimastigote up to 29.0 ± 3.8 μm in epimastigote cells found in the proventriculus (mean ± SD, with MAb25, Fig. S3 and Table S1). Although flagellum length variations followed the same trends as cell length, the amplitude was at least three times more pronounced, reaching a 1 to 10 ratio.

The presence and localization of four distinct components of the FAZ was examined by immunofluorescence. The FAZ-associated microtubule quartet was probed with the monoclonal antibody 1B41 that recognizes a particular isoform of β-tubulin (Gallo *et al*., 1988) (Fig. 4A). By immunofluorescence analysis, this antibody exclusively stains the quartet and does not produce a signal on any other microtubules (axonemal, sub-pellicular or mitotic microtubules). Antibodies recognizing three distinct components of the FAZ filament were used: L3B2 for the FAZ1 protein (Kohl *et al*., 1999) (Fig. S4), DOT1 for a distinct, yet unknown, protein (Woods *et al*., 1989; Kohl and Gull, 1998) (Fig. S5), and an antiserum against the FLA1 protein (Nozaki *et al*., 1996), recently shown to belong to the FAZ filament (B. Rotureau *et al*., unpubl. data). FAZ1 is a large repetitive protein only present in the FAZ that plays important roles in trypanosome cell division, but is not essential for assembly of the filament (Vaughan *et al*., 2008). FLA1 is a transmembrane protein whose extracellular domain is heavily glycosylated; its absence results in flagellum detachment in *T. brucei* (LaCount *et al*., 2002) and in the related parasite *Trypanosoma cruzi* (Cooper *et al*., 1993). All three proteins are tightly associated to the FAZ filament as they remain present after detergent extraction of the cytoskeleton. The anti-FLA1 and the anti-microtubule-quartet antibodies produced a positive signal in all stages (Fig. 4A). Measurements of the length of the FAZ filament based on these immunofluorescence images revealed an evolution correlated with the length of the flagellum (Fig. 4B and Table S1). The length of the FAZ ranged from 4.9 ± 2.4 μm in the short epimastigotes up to 22.9 ± 3.4 μm in mesocyclic cells (mean ± SD, $n = 289$ with the anti-FLA1 antibody) (Fig. 4B and Table S1). A close correlation was observed between the length of the FAZ filament and that of the quartet of microtubules (data not

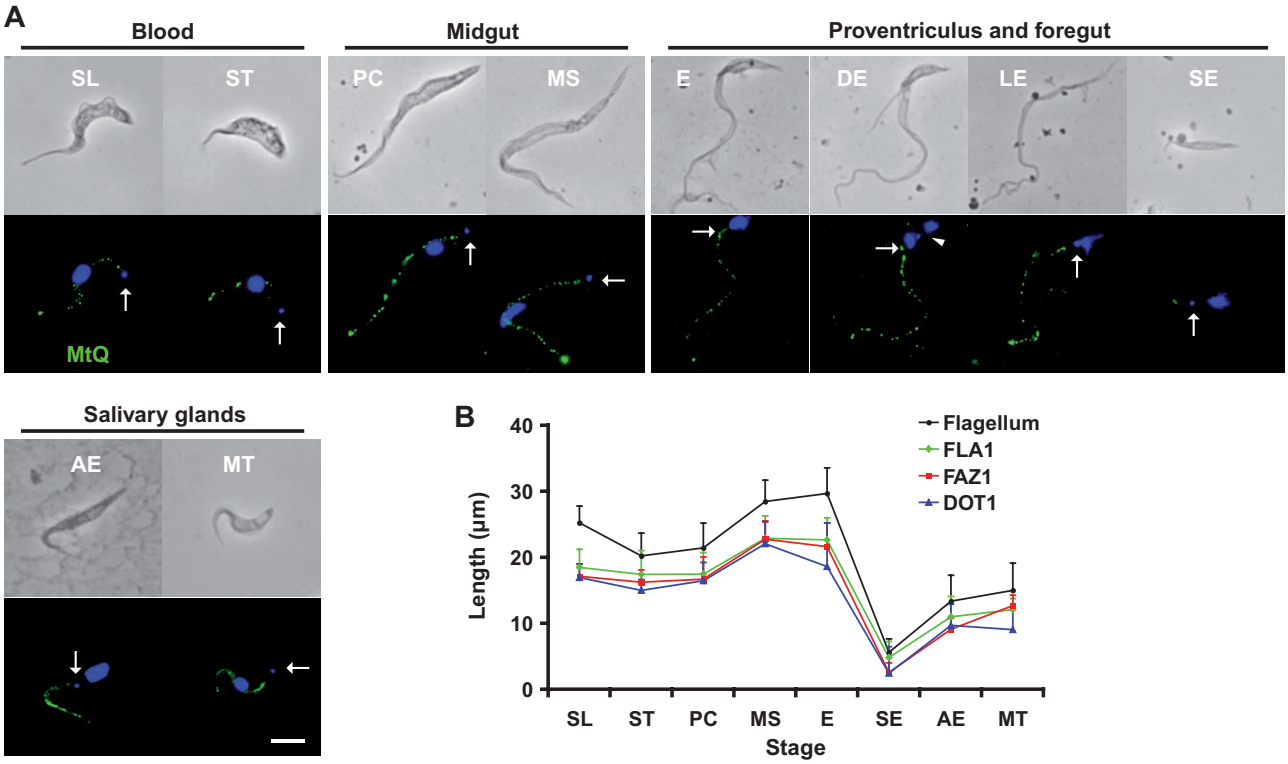

Fig. 4. The FAZ is present in all stages and its length follows that of the flagellum. Cells were fixed in methanol and stained with DAPI (blue in A) and the following antibodies.
A. Staining with the 1B41 antibody recognizing the microtubule quartet associated to the FAZ (MtQ in green). The scale bar represents 5 µm and the old (arrow) and new (arrowhead) basal body positions are indicated. Stages are presented in a chronological order and the name code is given in Fig. 1.
B. Staining with the MAb25 antibody targeting the axoneme, the antibody recognizing the transmembrane protein FLA1, or one of the two distinct markers of the FAZ filament L3B2 and DOT1. Length of the fluorescent signals was measured (Table S1) and presented as means ± SD (in µm) for each stage. Flagellar axoneme ($n = 307$), FLA1 ($n = 289$), FAZ1 ($n = 365$) and DOT1 ($n = 239$).

shown). However, from the beginning of nucleus migration towards the posterior end of the cell in the late mesocyclic stage, to the asymmetrically dividing epimastigote parasites, a dramatic reduction in the intensity of the fluorescent signal was observed for both the L3B2 and DOT1 probes. Comparison of parasites from the proventriculus in the same microscope field showed a dramatic drop in signal intensity for both L3B2 (80%, $n = 65$) and DOT1 (82%, $n = 28$) in long epimastigotes and dividing epimastigotes compared with mesocyclic trypomastigotes, which exhibited a signal intensity similar to that of procyclic trypomastigotes (Fig. 5C–F). The signal became detectable again associated to the FAZ in close vicinity of the flagellum in short epimastigote cells and in all subsequent stages (Figs S4 and S5). In contrast, single or simultaneous immuno-labelling of FLA1 or the four FAZ-associated microtubules remained unchanged in all proventricular stages (Fig. 5A, B and F). These data reveal important remodelling of the FAZ filament during the transition from the trypomastigote to the epimastigote configuration.

Discussion

In this study, we investigated the evolution of the cytoskeleton and of the flagellar apparatus during trypanosome differentiation in the tsetse fly. First, we confirmed that all previously characterized parasite stages could be identified in our hands, although the chronology of events was shifted by about 1 week compared with published reports (Van Den Abbeele *et al.*, 1999; Peacock *et al.*, 2007; Sharma *et al.*, 2008; Oberle *et al.*, 2010). Nevertheless, measurement of parasite length at various stages of infection was in good agreement with data from the literature (Van Den Abbeele *et al.*, 1999; Sharma *et al.*, 2008).

Cytoskeleton dynamics and cell volume evolution

As in many protists, the trypanosome cytoskeleton is not depolymerized during mitosis. Instead, a complete microtubule corset is inherited by each daughter cell in a semi-conservative manner, as shown in cultured procyclic cells (Sherwin and Gull, 1989b). Tubulin and acetylated

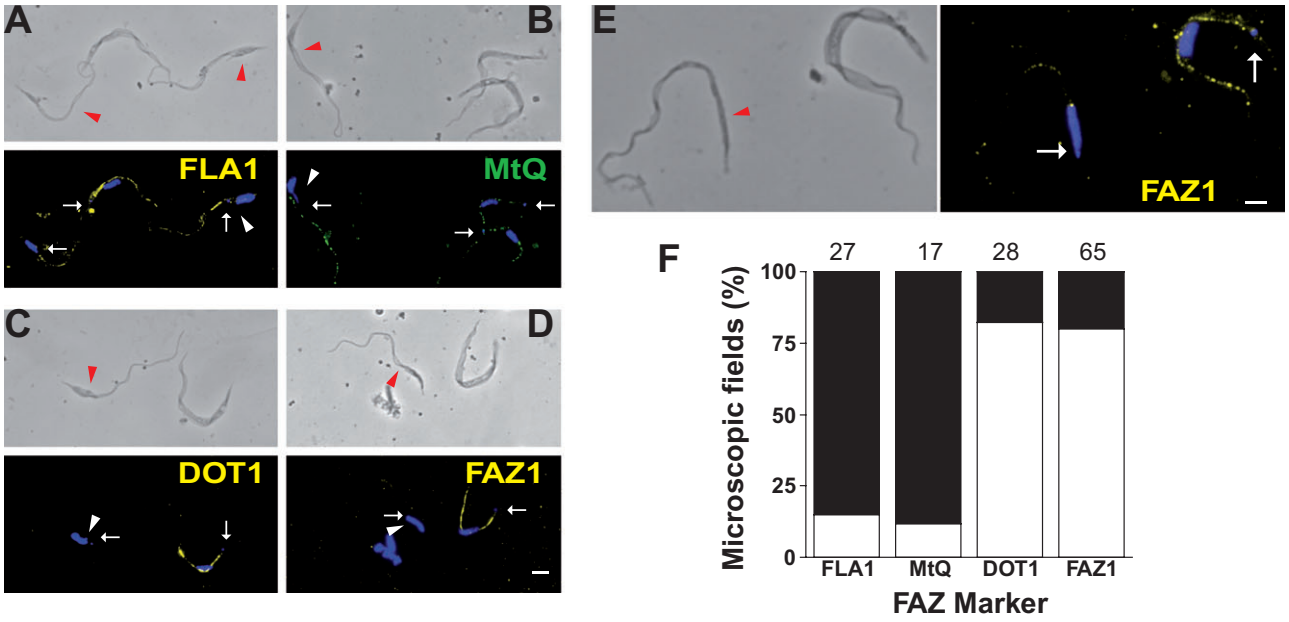

Fig. 5. Remodelling of the FAZ filament during differentiation in the proventriculus. Cells were fixed in methanol and stained with DAPI (blue in A–E), the antibody recognizing the transmembrane protein FLA1 (A, yellow), the 1B41 antibody targeting the MtQ (B, green), and two distinct markers of the FAZ filament DOT1 (C, yellow) and L3B2 (D and E, yellow). A–E. The scale bars represent 5 μm and the old (white arrow) and new (white arrowhead) basal body positions are indicated. Epimastigote cells are shown with red arrowheads.
F. The intensity of the signals obtained for the anti-FLA1, 1B41, L3B2 and DOT1 were compared between proventricular forms of the parasites in the same microscope fields. The occurrence of an equal or lower (black bars) or higher (white bars) fluorescent signal in mesocyclic cells compared with epimastigotes/dividing epimastigotes were counted and plotted as percentage of the total number of fields observed (*n* at the top of the bars).

α-tubulin staining confirmed the existence of the corset at all investigated stages. We have exploited this feature to set up a novel method to estimate cell volume. To our knowledge, estimations of the *T. brucei* cell volume have only been reported for bloodstream stages, in culture (Grunfelder *et al*., 2002) or isolated from infected rats (Opperdoes *et al*., 1984; Reuner *et al*., 1997). Our cell volume calculations (45 and 53 μm^3 for slender and stumpy cells, respectively) are close to the previously published estimations: 36 μm^3 obtained by electronic pulse area analysis (Reuner *et al*., 1997), 52 μm^3 calculated by stereological analysis of electron microscopic images (Grunfelder *et al*., 2002), 58 μm^3 estimated by the inulin exclusion method (Opperdoes *et al*., 1984) and 59 μm^3 evaluated in 3D microscopic images of fluorescent living cells (Grunfelder *et al*., 2002), validating our approach.

Tyrosinated α-tubulin is a recognized marker of recently assembled tubulin and was used in cultured procyclic trypanosomes to monitor microtubule dynamics during the cell cycle, revealing elongation of microtubules at the posterior end and intercalation of new microtubules within the existing network (Sherwin *et al*., 1987; Sherwin and Gull, 1989b). We confirmed these data on procyclic parasites obtained from the midgut and showed that all three proliferative stages (bloodstream form, procyclic stage and attached epimastigote) exhibit microtubule elongation at the posterior end, a process coupled to a significant increase in total cell volume.

Cytoskeleton elongation at the posterior end is also a feature of two differentiating stages: stumpy to procyclic (Matthews *et al*., 1995) and procyclic to mesocyclic (Hammarton *et al*., 2004). These two steps involve increase in cell length but modest increase in cell volume. In sharp contrast, no apparent increase in tubulin polymerization was observed during the thinning of the cell body and the nucleus migration occurring from the pre-epimastigote to the epimastigote stage in the proventriculus. Cell volume did not increase either before cytokinesis in asymmetrically dividing epimastigotes. Once anaphase is clearly initiated, the posterior end appears more dilated and becomes brightly positive for tyrosinated tubulin, a staining that encompasses the two nuclei. These changes indicate the dynamic formation of new microtubules and/or the remodelling of existing ones. This is the first observation of tubulin tyrosination without posterior elongation in trypanosomes. This could imply a depolymerization of some sub-pellicular microtubules before assembly in a new configuration, a phenomenon compatible with the observed stability of the cell volume. This could be related to the formation of a much smaller daughter cell (the short epimastigote) at the asymmetric division and to the assembly of a very short flagellum.

Roles of the FAZ in trypanosome development in the tsetse fly

The morphometric measurements produced here demonstrate that the evolution of cell length is more closely related to variations in flagellum length than in cell volume. In cultured procyclic trypanosomes, morphogenesis has been shown to be associated to flagellum length (Kohl *et al*., 2003). The FAZ has been proposed to define the position and the direction of the cleavage furrow, hence defining morphogenesis (Robinson *et al*., 1995). Intraflagellar transport RNAi mutants undergo an asymmetric division with the formation of a cell of normal length inheriting the normal old flagellum/FAZ and a short cell inheriting the short new flagellum/FAZ, with a direct correlation with flagellum length (Kohl *et al*., 2003). As it has previously been hypothesized (Sharma *et al*., 2008), such a mechanism could explain the asymmetric division observed in epimastigotes of the proventriculus. A second postulated function of the FAZ is the control of basal body and flagellar pocket positioning (Absalon *et al*., 2007; Bonhivers *et al*., 2008a). Tomography studies showed that the microtubule quartet wraps around the flagellar pocket and that the FAZ filament is in close contact with the collar of the flagellar pocket (Lacomble *et al*., 2009). An involvement of the FAZ in basal body positioning is further supported by the location of the basal body at the extreme posterior end of the cell in the *BILBO1*^{RNAi} mutant that lacks the flagellar pocket collar and fails to assemble a new FAZ (Bonhivers *et al*., 2008b).

In cultured procyclic cells, the FAZ elongates at the same rate as the flagellum (Kohl *et al*., 1999). Our data show that the molecular composition of the FAZ, with a typical dotty pattern along the adhesion region, is conserved over the parasite development in the tsetse fly, despite the exhaustive modifications of flagellum length. One striking exception to this rule is the differentiation from the mesocyclic trypomastigote to the epimastigote form. This transition results from a thinning of the cell body and a relative movement of the nucleus towards the posterior end of the cell, and occurs at the same time as the initiation of mitosis (Sharma *et al*., 2008). We revealed that a remodelling of the FAZ filament initiates as soon as the elongated nucleus starts its migration towards the posterior end. The protein FAZ1 and the distinct antigen recognized by the monoclonal antibody DOT1 (Kohl and Gull, 1998) fell below detection level whereas neighbouring mesocyclic parasites were still positive. This could be due to either absence of these two proteins, or to reduced accessibility to the epitopes that could result from post-translational modifications or changes in molecular configuration, but in any case, it reveals a modification in FAZ filament organization. It should be reminded here that FAZ1 is not required for the construction of the FAZ filament *per se* (Vaughan *et al*., 2008). As working model, we propose that this re-organization is related to the movement of the nucleus in a more posterior position. Indeed, treatment of extracted trypanosome cytoskeletons with calcium depolymerizes the sub-pellicular microtubules, leaving behind only the flagellum, the FAZ filament and the nucleus that appears to be associated with the filament (Absalon *et al*., 2007). Thus, we suggest that the observed changes in molecular disposition of the FAZ filament could somehow liberate and/or guide the nucleus for posterior migration, for example by the action of motors that remain to be identified. These could be associated to the microtubule quartet of the FAZ that remains present in these cells.

In contrast to the differentiation between bloodstream stumpy and midgut procyclic stages, which occurs during a G1 arrest (Matthews and Gull, 1994), the differentiation of mesocyclic trypomastigotes to epimastigotes occurs at the beginning of the asymmetric cell division cycle (Van Den Abbeele *et al*., 1999; Sharma *et al*., 2008). We observed that both L3B2 and DOT1 markers were recovered after the asymmetric division in the short epimastigote daughter cells but not in the long siblings. This observation is in accordance with the fact that the long epimastigote daughter cell does not enter S-phase, as judged by the lack of expression of the cohesin component SCC1, and is likely to degenerate as many are observed with diffuse or dispersed nuclear staining (Sharma *et al*., 2008). Further understanding of the role of the FAZ in these important morphogenetic processes awaits the identification of novel molecular components for functional investigation. It should be stressed that all FAZ components identified so far are specific to trypanosomatid parasites and could represent promising drug target in the future given the essential role of this sub-cellular structure.

Our results bring molecular evidence for cytoskeleton shaping that takes place during trypanosome differentiation. Several functions could be proposed to link the specific morphological and molecular modifications with trypanosome behaviour, alongside previously published observations (Vickerman *et al*., 1988; Van Den Abbeele *et al*., 1999; Peacock *et al*., 2007; Sharma *et al*., 2008; Oberle *et al*., 2010). First, the high motility of procyclic trypomastigotes found in the posterior midgut could be involved in crossing of the peritrophic membrane that separates the blood meal from the midgut epithelium, hence escaping the more aggressive environment of the gut lumen. Their proliferative status is linked to the early settlement and amplification of the parasite population, and subsequently, with the maintenance of the midgut infection during the whole life of the vector. In contrast, cells at the mesocyclic stage do not show signs of proliferation but are longer and thinner. These elongated

parasites swim together sometimes at high density (B. Rotureau *et al*., unpubl. data) all along the midgut, from its posterior part to the proventriculus. Such a characteristic shape could remarkably fit their migratory function. Then, the relatively long journey of epimastigote parasites to the salivary gland implies passage via the foregut and the hypopharynx, and finally through the narrow salivary gland duct. The few but long, thin and highly motile dividing epimastigote parasites found in these regions could be well-adapted to deliver free short epimastigote cells, whose motility properties appear more limited, directly in the salivary glands. In these conditions, the elongated shape might offer less friction and facilitate migration. Anterior positioning of the flagellum in short epimastigotes could be explained by the necessity for adhesion to the salivary gland epithelium, as these parasites are not yet infective: they do not possess the VSG coat but display a specific cell surface protein called BARP (Urwyler *et al*., 2007). Proliferation of attached epimastigotes is likely required to ensure colonization of the epithelium and sustained production of infective parasites in the saliva. After their attachment to the epithelium, epimastigotes elongate their posterior end, adopting characteristic protrusions. As the flagellum is attached, these protusions oscillating in the lumen offer a significant surface that could be involved in sensing and/or molecular exchanges with the environment. Upon release in the saliva, free infective metacyclic trypomastigotes are shaped like bloodstream forms and possess a VSG coat but are small enough to travel through the narrow ducts of the tsetse mouthparts. The trypomastigote morphotype could ensure more efficient swimming in a crowded environment such as encountered in the blood with millions of erythrocytes (Engstler *et al*., 2007). In all cases, the flagellum tracts the cell forward, with its tip always extending beyond the cell body. Such a configuration would ensure that the tip of this organelle is the first one to be in contact with new environments, making it a strong sensing candidate (Rotureau *et al*., 2009). These are only conjectures but it emphasizes the link between the multiple cytoskeletal modifications, including those of the flagellum, and the adequate functions of each trypanosome stage in its specific environment in the insect.

Experimental procedures

Trypanosome strain and cultures

The pleomorphic strain *Trypanosoma brucei brucei* AnTat1.1 (Le Ray *et al*., 1977) was used throughout this study. Slender bloodstream parasites were cultured in HMI9 medium supplemented with 10% foetal bovine serum (Hirumi and Hirumi, 1989). Alternatively, they were plated on solid HMI9 medium supplemented with 10% fetal bovine serum to induce their differentiation into the stumpy form (Carruthers and Cross, 1992; Vassella *et al*., 1997). Stumpy parasites were then triggered to differentiate into the procyclic culture form in DTM medium containing 20% fetal bovine serum by the addition of 6 mM *cis*-aconitate and a temperature shift from 37°C to 27°C (Brun and Schonenberger, 1981). Procyclic trypanosomes were maintained in SDM79 medium (Brun and Schonenberger, 1979) supplemented with 10% fetal bovine serum and 20 mM glycerol.

Tsetse fly infection, maintenance and dissection

Teneral males of *Glossina morsitans morsitans* from 8 to 96 h post-eclosion were obtained from the 'TRYPANOSOM' UMR177 IRD-CIRAD, Campus International de Baillarguet, Montpellier, France. Tsetse flies were allowed to ingest parasites in culture medium during their first meal through a silicone membrane. We used either (i) stumpy cells at 10^6 cells per millilitre in HMI9 medium supplemented with 10% foetal bovine serum, 60 mM N-acetylglucosamine (Peacock *et al*., 2006) and 2.5% (w/v) bovine serum albumin (Kabayo *et al*., 1986), or (ii) procyclic cultured trypanosomes at 5.10^6 cells per millilitre in SDM79 medium supplemented with 10% foetal bovine serum, 60 mM N-acetylglucosamine (Peacock *et al*., 2006) and 2.5% (w/v) bovine serum albumin (Kabayo *et al*., 1986). Tsetse flies were subsequently maintained in Roubaud cages at 27°C and 70% hygrometry and fed twice a week through a silicone membrane with fresh rabbit blood in heparin.

Flies were starved for at least 48 h before being dissected at different time points from 14 to 55 days after ingestion of the infected meal. Salivary glands were first dissected into a drop of PBS or SDM79 medium. Whole tsetse alimentary tracts, from the distal part of the foregut to the rectum, were then dissected and arranged lengthways for assessment of parasite presence. Foregut and proventriculus were physically separated from the midgut in distinct PBS/SDM79 drops. Tissues were dilacerated and recovered parasites were treated for further experiments no more than 15 min after dissection.

Immunofluorescence

For immunofluorescence, cells were washed in PBS or SDM79 medium, settled on poly-L-lysine coated or uncoated slides and fixed in 4% para-formaldehyde (PFA) for 10 min. Fixed cells were permeabilized with 0.5% Nonidet P-40 in PBS for 10 min and samples were rinsed to remove the excess of detergent. Blocking was performed by an incubation of 45 min in PBS containing 1% bovine serum albumin. Alternatively, cells were fixed in methanol at –20°C for at least 5 min and re-hydrated in PBS for 10 min. In all cases, slides were incubated with primary antibodies for 60 min at room temperature. They were washed and incubated with the appropriate secondary antibodies coupled to Alexa 488 (Invitrogen) or Cy3 (Jackson). Slides were stained with DAPI for visualization of kinetoplast and nuclear DNA content, and mounted under cover slips with ProLong antifade reagent (Invitrogen).

The TAT1 (IgG2b) (Woods *et al*., 1989) antibody recognizes α-tubulin. MAb25 (IgG2a) labels a protein found all along the axoneme (Pradel *et al*., 2006), while the monoclonal antibody L8C4 (IgG1) specifically recognizes PFR2, localized throughout the PFR (Kohl *et al*., 1999). The YL1/2 antibody (IgG) (Kilmartin *et al*., 1982) labels tyrosinated α-tubulin while the C3B9 antibody

(IgG2b) detects acetylated α-tubulin (Woods *et al*., 1989). Concerning the FAZ components, a polyclonal antibody was used to stain the transmembrane protein FLA1 (Nozaki *et al*., 1996), the 1B41 antibody recognizes the microtubule quartet associated to the FAZ filament (Gallo *et al*., 1988), and the two markers of the FAZ filament L3B2 (Kohl *et al*., 1999) and DOT1 (Woods *et al*., 1989), respectively, target FAZ1 and a distinct yet unknown protein (Kohl and Gull, 1998). For each antibody, IFA experiments were repeated on trypanosomes issued from 3 to 13 different flies and from at least 3 distinct experimental infections.

Measurements and analyses

Samples were observed either with (i) a DMR microscope (Leica) and images were captured with a CoolSnap HQ camera (Roper Scientific) (ii) with a DMI4000 microscope (Leica) and images were acquired with a Retiga-SRV camera (Q39 Imaging) or (iii) with a digital D-Eclipse EZ-C1si confocal system (Nikon) installed on an Eclipse TE2000-E inverted microscope (Nikon). Pictures were analysed and cell parameters were measured using the IPLab Spectrum 3.9 software (Scanalytics & BD Biosciences), the ImageJ 1.38X software (NIH) or the NIS-elements software (Nikon). For clarity purposes, brightness and contrast of several pictures presented in figures were adjusted after their analysis in accordance with editorial policies. The scale bars represent 5 μm in all figures. The cell volumes were calculated from *in silico* 3D reconstructions of 200 nm confocal z-stack pictures of PFA-fixed cells stained with TAT1. Calculations were done in the ImageJ-derived Fiji package after an 'intermodes' auto-threshold normalization of the fluorescence. Statistical analyses and plots were performed in Excel or with the KaleidaGraph V.4.0 software (Synergy Software). Lengths (μm) and volumes (μm^3) were plotted as means ± SD. One-way ANOVA tests were performed with intergroup comparisons between two consecutive stages by Tukey *ad hoc* post-tests with $a = 0.05$ and significant results were indicated with $^{*}P < 0.0001$, $^{**}P < 0.001$ and $^{***}P < 0.01$ (Fig. 2).

Acknowledgements

We thank B. Tchicaya and J. Janelle from the UMR177 IRD-CIRAD team headed by G. Cuny (Montpellier, France) for generously providing tsetse flies. We are grateful to J. Van Den Abbeele for providing the trypanosome AnTat 1.1 cell line. We acknowledge L. Kohl, D. Robinson and K. Gull for providing various antibodies. We thank P. Reiter and A. Scherf for providing access to the insectarium and to the confocal microscope respectively. We thank G. Milon, D. Julkowska, G. Spaeth, F. Bringaud and D. Robinson for critical reading of the manuscript. This work was funded by the CNRS, the Institut Pasteur and by a MIE grant from the ANR. BR is funded by a Roux post-doctoral fellowship from the Institut Pasteur and IS by a FNR fellowship. The authors declare no competing financial interests.

References

Absalon, S., Kohl, L., Branche, C., Blisnick, T., Toutirais, G., Rusconi, F., *et al*. (2007) Basal body positioning is controlled by flagellum formation in *Trypanosoma brucei*. *PLoS ONE* **2:** e437.

Bonhivers, M., Landrein, N., Decossas, M., and Robinson, D.R. (2008a) A monoclonal antibody marker for the exclusion-zone filaments of *Trypanosoma brucei*. *Parasit Vectors* **1:** 21.

Bonhivers, M., Nowacki, S., Landrein, N., and Robinson, D.R. (2008b) Biogenesis of the trypanosome endo-exocytotic organelle is cytoskeleton mediated. *PLoS Biol* **6:** e105.

Brun, R., and Schonenberger, M. (1979) Cultivation and in vitro cloning or procyclic culture forms of *Trypanosoma brucei* in a semi-defined medium. Short communication. *Acta Trop* **36:** 289–292.

Brun, R., and Schonenberger, M. (1981) Stimulating effect of citrate and cis-Aconitate on the transformation of *Trypanosoma brucei* bloodstream forms to procyclic forms in vitro. *Z Parasitenkd* **66:** 17–24.

Brun, R., Blum, J., Chappuis, F., and Burri, C. (2009) Human African trypanosomiasis. *Lancet* **375:** 148–159.

Carruthers, V.B., and Cross, G.A. (1992) High-efficiency clonal growth of bloodstream- and insect-form *Trypanosoma brucei* on agarose plates. *Proc Natl Acad Sci USA* **89:** 8818–8821.

Cooper, R., de Jesus, A.R., and Cross, G.A. (1993) Deletion of an immunodominant *Trypanosoma cruzi* surface glycoprotein disrupts flagellum-cell adhesion. *J Cell Biol* **122:** 149–156.

Davidge, J.A., Chambers, E., Dickinson, H.A., Towers, K., Ginger, M.L., McKean, P.G., and Gull, K. (2006) Trypanosome IFT mutants provide insight into the motor location for mobility of the flagella connector and flagellar membrane formation. *J Cell Sci* **119:** 3935–3943.

Engstler, M., Pfohl, T., Herminghaus, S., Boshart, M., Wiegertjes, G., Heddergott, N., and Overath, P. (2007) Hydrodynamic flow-mediated protein sorting on the cell surface of trypanosomes. *Cell* **131:** 505–515.

Fenn, K., and Matthews, K.R. (2007) The cell biology of *Trypanosoma brucei* differentiation. *Curr Opin Microbiol* **10:** 539–546.

Gallo, J.M., Precigout, E., and Schrevel, J. (1988) Subcellular sequestration of an antigenically unique beta-tubulin. *Cell Motil Cytoskeleton* **9:** 175–183.

Grunfelder, C.G., Engstler, M., Weise, F., Schwarz, H., Stierhof, Y.D., Boshart, M., and Overath, P. (2002) Accumulation of a GPI-anchored protein at the cell surface requires sorting at multiple intracellular levels. *Traffic* **3:** 547–559.

Gull, K. (1999) The cytoskeleton of trypanosomatid parasites. *Annu Rev Microbiol* **53:** 629–655.

Hammarton, T.C., Engstler, M., and Mottram, J.C. (2004) The *Trypanosoma brucei* cyclin, CYC2, is required for cell cycle progression through G1 phase and for maintenance of procyclic form cell morphology. *J Biol Chem* **279:** 24757–24764.

Hirumi, H., and Hirumi, K. (1989) Continuous cultivation of *Trypanosoma brucei* blood stream forms in a medium containing a low concentration of serum protein without feeder cell layers. *J Parasitol* **75:** 985–989.

Hoare, C.A., and Wallace, F.G. (1966) Developmental Stages of Trypanosomatid Flagellates: a New Terminology. *Nature* **212:** 1385–1386.

Kabayo, J.P., DeLoach, J.R., Spates, G.E., Holman, G.M., and Kapatsa, G.M. (1986) Studies on the biochemical

basis of the nutritional quality of tsetse fly diets. *Comp Biochem Physiol A Comp Physiol* **83:** 133–139.
Kilmartin, J.V., Wright, B., and Milstein, C. (1982) Rat monoclonal antitubulin antibodies derived by using a new nonsecreting rat cell line. *J Cell Biol* **93:** 576–582.
Kohl, L., and Gull, K. (1998) Molecular architecture of the trypanosome cytoskeleton. *Mol Biochem Parasitol* **93:** 1–9.
Kohl, L., Sherwin, T., and Gull, K. (1999) Assembly of the paraflagellar rod and the flagellum attachment zone complex during the *Trypanosoma brucei* cell cycle. *J Eukaryot Microbiol* **46:** 105–109.
Kohl, L., Robinson, D., and Bastin, P. (2003) Novel roles for the flagellum in cell morphogenesis and cytokinesis of trypanosomes. *EMBO J* **22:** 5336–5346.
Lacomble, S., Vaughan, S., Gadelha, C., Morphew, M.K., Shaw, M.K., McIntosh, J.R., and Gull, K. (2009) Three-dimensional cellular architecture of the flagellar pocket and associated cytoskeleton in trypanosomes revealed by electron microscope tomography. *J Cell Sci* **122:** 1081–1090.
LaCount, D.J., Barrett, B., and Donelson, J.E. (2002) *Trypanosoma brucei* FLA1 is required for flagellum attachment and cytokinesis. *J Biol Chem* **277:** 17580–17588.
Le Ray, D., Barry, J.D., Easton, C., and Vickerman, K. (1977) First tsetse fly transmission of the 'AnTat' serodeme of *Trypanosoma brucei*. *Ann Soc Belg Med Trop* **57:** 369–381.
Matthews, K.R., and Gull, K. (1994) Evidence for an interplay between cell cycle progression and the initiation of differentiation between life cycle forms of African trypanosomes. *J Cell Biol* **125:** 1147–1156.
Matthews, K.R., Sherwin, T., and Gull, K. (1995) Mitochondrial genome repositioning during the differentiation of the African trypanosome between life cycle forms is microtubule mediated. *J Cell Sci* **108** (Part 6)**:** 2231–2239.
Moreira-Leite, F.F., Sherwin, T., Kohl, L., and Gull, K. (2001) A trypanosome structure involved in transmitting cytoplasmic information during cell division. *Science* **294:** 610–612.
Nozaki, T., Haynes, P.A., and Cross, G.A. (1996) Characterization of the *Trypanosoma brucei* homologue of a *Trypanosoma cruzi* flagellum-adhesion glycoprotein. *Mol Biochem Parasitol* **82:** 245–255.
Oberle, M., Balmer, O., Brun, R., and Roditi, I. (2010) Bottlenecks and the maintenance of minor genotypes during the life cycle of *Trypanosoma brucei*. *PLoS Pathog* **6:** e1001023.
Opperdoes, F.R., Baudhuin, P., Coppens, I., De Roe, C., Edwards, S.W., Weijers, P.J., and Misset, O. (1984) Purification, morphometric analysis, and characterization of the glycosomes (microbodies) of the protozoan hemoflagellate *Trypanosoma brucei*. *J Cell Biol* **98:** 1178–1184.
Peacock, L., Ferris, V., Bailey, M., and Gibson, W. (2006) Multiple effects of the lectin-inhibitory sugars d-glucosamine and N-acetyl-glucosamine on tsetse-trypanosome interactions. *Parasitology* **132:** 651–658.
Peacock, L., Ferris, V., Bailey, M., and Gibson, W. (2007) Dynamics of infection and competition between two strains of *Trypanosoma brucei* brucei in the tsetse fly observed using fluorescent markers. *Kinetoplastid Biol Dis* **6:** 4.
Portman, N., and Gull, K. (2009) The paraflagellar rod of kinetoplastid parasites: from structure to components and function. *Int J Parasitol* **40:** 135–148.
Pradel, L.C., Bonhivers, M., Landrein, N., and Robinson, D.R. (2006) NIMA-related kinase TbNRKC is involved in basal body separation in *Trypanosoma brucei*. *J Cell Sci* **119:** 1852–1863.
Ralston, K.S., Kabututu, Z.P., Melehani, J.H., Oberholzer, M., and Hill, K.L. (2009) The *Trypanosoma brucei* flagellum: moving parasites in new directions. *Annu Rev Microbiol* **63:** 335–362.
Reuner, B., Vassella, E., Yutzy, B., and Boshart, M. (1997) Cell density triggers slender to stumpy differentiation of *Trypanosoma brucei* bloodstream forms in culture. *Mol Biochem Parasitol* **90:** 269–280.
Robinson, D.R., and Gull, K. (1991) Basal body movements as a mechanism for mitochondrial genome segregation in the trypanosome cell cycle. *Nature* **352:** 731–733.
Robinson, D.R., Sherwin, T., Ploubidou, A., Byard, E.H., and Gull, K. (1995) Microtubule polarity and dynamics in the control of organelle positioning, segregation, and cytokinesis in the trypanosome cell cycle. *J Cell Biol* **128:** 1163–1172.
Roditi, I., and Lehane, M.J. (2008) Interactions between trypanosomes and tsetse flies. *Curr Opin Microbiol* **11:** 345–351.
Rotureau, B., Morales, M.A., Bastin, P., and Spath, G.F. (2009) The flagellum-MAP kinase connection in Trypanosomatids: a key sensory role in parasite signaling and development? *Cell Microbiol* **11:** 710–718.
Schneider, A., Sherwin, T., Sasse, R., Russell, D.G., Gull, K., and Seebeck, T. (1987) Subpellicular and flagellar microtubules of *Trypanosoma brucei* brucei contain the same alpha-tubulin isoforms. *J Cell Biol* **104:** 431–438.
Sharma, R., Peacock, L., Gluenz, E., Gull, K., Gibson, W., and Carrington, M. (2008) Asymmetric cell division as a route to reduction in cell length and change in cell morphology in trypanosomes. *Protist* **159:** 137–151.
Sharma, R., Gluenz, E., Peacock, L., Gibson, W., Gull, K., and Carrington, M. (2009) The heart of darkness: growth and form of *Trypanosoma brucei* in the tsetse fly. *Trends Parasitol* **25:** 517–524.
Sherwin, T., and Gull, K. (1989a) The cell division cycle of *Trypanosoma brucei* brucei: timing of event markers and cytoskeletal modulations. *Philos Trans R Soc Lond B Biol Sci* **323:** 573–588.
Sherwin, T., and Gull, K. (1989b) Visualization of detyrosination along single microtubules reveals novel mechanisms of assembly during cytoskeletal duplication in trypanosomes. *Cell* **57:** 211–221.
Sherwin, T., Schneider, A., Sasse, R., Seebeck, T., and Gull, K. (1987) Distinct localization and cell cycle dependence of COOH terminally tyrosinolated alpha-tubulin in the microtubules of *Trypanosoma brucei* brucei. *J Cell Biol* **104:** 439–446.
Simarro, P.P., Jannin, J., and Cattand, P. (2008) Eliminating human African trypanosomiasis: where do we stand and what comes next? *PLoS Med* **5:** e55.
Urwyler, S., Studer, E., Renggli, C.K., and Roditi, I. (2007) A family of stage-specific alanine-rich proteins on the surface of epimastigote forms of *Trypanosoma brucei*. *Mol Microbiol* **63:** 218–228.
Van Den Abbeele, J., Claes, Y., van Bockstaele, D., Le Ray, D., and Coosemans, M. (1999) *Trypanosoma brucei* spp.

development in the tsetse fly: characterization of the post-mesocyclic stages in the foregut and proboscis. *Parasitology* **118** (Part 5)**:** 469–478.
Vassella, E., Reuner, B., Yutzy, B., and Boshart, M. (1997) Differentiation of African trypanosomes is controlled by a density sensing mechanism which signals cell cycle arrest via the cAMP pathway. *J Cell Sci* **110** (Part 21)**:** 2661–2671.
Vaughan, S. (2010) Assembly of the flagellum and its role in cell morphogenesis in *Trypanosoma brucei*. *Curr Opin Microbiol* **13:** 453–458.
Vaughan, S., Kohl, L., Ngai, I., Wheeler, R.J., and Gull, K. (2008) A Repetitive Protein Essential for the Flagellum Attachment Zone Filament Structure and Function in *Trypanosoma brucei*. *Protist* **159:** 127–136.
Vickerman, K., Tetley, L., Hendry, K.A., and Turner, C.M. (1988) Biology of African trypanosomes in the tsetse fly. *Biol Cell* **64:** 109–119.
Woods, A., Sherwin, T., Sasse, R., MacRae, T.H., Baines, A.J., and Gull, K. (1989) Definition of individual components within the cytoskeleton of *Trypanosoma brucei* by a library of monoclonal antibodies. *J Cell Sci* **93** (Part 3)**:** 491–500.
Woodward, R., and Gull, K. (1990) Timing of nuclear and kinetoplast DNA replication and early morphological events in the cell cycle of *Trypanosoma brucei*. *J Cell Sci* **95** (Part 1)**:** 49–57.

Supporting information

Additional Supporting Information may be found in the online version of this article:

Fig. S1. Distribution of tyrosinated α-tubulin in parasite stages found in mammalian bloodstream and tsetse midgut. Cells were fixed in methanol and stained with DAPI (blue) and the YL1/2 antibody (green) recognizing α-tyrosinated tubulin. The scale bar represents 5 μm and the basal body position is indicated with an arrow. Stages are presented in a chronological order and the name code is given in Fig. 1.
Fig. S2. Distribution of acetylated and tyrosinated α-tubulin during asymmetric division in 2K2N dividing epimastigotes observed by epifluorescence and confocal microscopy. Proventricular cells were fixed in methanol (epifluorescence) or in PFA (confocal) and stained with DAPI (red) and the YL1/2 antibody (green) recognizing tyrosinated tubulin or the C3B9 antibody (green) labelling acetylated tubulin. The scale bar represents 5 μm and the old (arrow) and new (arrowhead) basal body positions are indicated.
Fig. S3. Flagellar axoneme and PFR2 localization and length variations during trypanosome development. The 10 main morphological stages of the *T. brucei* parasite cycle were fixed in methanol and stained with DAPI (blue in A), the L8C4 antibody recognizing the PFR2 protein (green in A) or the mAb25 antibody labelling the axoneme (not shown). The scale bar represents 5 μm and the old (arrow) and new (arrowhead) basal body positions are indicated. Stages are presented in a chronological order and the name code is given in Fig. 1.
B. Variations (mean ± SD in μm) of flagellum length measured on phase contrast pictures ('Flagellum', $n = 1221$), or upon L8C4 ('PFR', $n = 218$) or MAb25 staining ('axoneme', $n = 307$), compared with the evolution of total trypanosome length from the tip of the flagellum to the posterior end of cell (Total, $n = 1273$).
Fig. S4. FAZ1 localization during trypanosome development. The 10 main morphological stages of the *T. brucei* parasite cycle were fixed in methanol and stained with DAPI (blue) and the L3B2 antibody (green) labelling FAZ1. Note that the FAZ1 labelling is present in all stages, except in epimastigotes and dividing epimastigotes in the proventriculus. In these stages, the fluorescent signal is absent, or is restricted to a few areas of reduced intensity. The scale bar represents 5 μm and the old (arrow) and new (arrowhead) basal body positions are indicated. Stages are presented in a chronological order and the name code is given in Fig. 1.
Fig. S5. Localization of the antigen recognized by the DOT1 marker during trypanosome development. The 10 main morphological stages of the *T. brucei* parasite cycle were fixed in methanol and stained with DAPI (blue) and the DOT1 antibody (green). Note that the DOT1 labelling is present in all stages, except in epimastigotes and dividing epimastigotes in the proventriculus. As for L3B2, the fluorescent signal is absent, or is restricted to a few areas of reduced intensity. The scale bar represents 5 μm and the old (arrow) and new (arrowhead) basal body positions are indicated. Stages are presented in a chronological order and the name code is given in Fig. 1.
Table S1. Morphometric measurements in trypanosome stages. The main morphological stages of the *T. brucei* parasite cycle were fixed in methanol and stained with DAPI and various antibodies (cf. section *Experimental procedures*). This table summarizes all the morphometric measurements performed in the present study in 1K1N parasites. The mean lengths ± SD, ranges and numbers of cells studied are given in μm for nine parameters: the total length of the cell from the tip of the flagellum to the posterior end of the cell (Total), the length of the flagellum in phase contrast pictures (Flagellum), the distance between the centre of the nucleus and the kinetoplast (N–K), the distance between the centre of the nucleus and the posterior end of cell (N-Post), the lengths of the fluorescent signals observed after staining of FLA1, FAZ1 (even in E when it was possible), DOT1 (even in E and DE when it was possible), PFR2 and the axoneme. A total of 1276 parasites was analysed. Stages are presented in a chronological order and the name code is given in Fig. 1.

Please note: Wiley-Blackwell are not responsible for the content or functionality of any supporting materials supplied by the authors. Any queries (other than missing material) should be directed to the corresponding author for the article.